



The high temperature degradation of ferritic stainless steel in solid carbon atmospheres

Prakeaw NGAMSRI¹, Suwijak POKWITDKUL¹, Paweena TREEWIRIYAKITJA^{1,2}, Pempisuth THONGYOU³, Ratchapon NILPRAPA¹, and Jennarong TUNGTRONGPAIROJ^{1,*}

¹ High Temperature Corrosion Research Centre, Department of Materials and Production Technology Engineering, Faculty of Engineering, King Mongkut's University of Technology North Bangkok, 1518 Pracharat 1 Road, Wongsawang, Bangsue, Bangkok 10800, Thailand

² Corrosion Technology Department, Thai-French Innovation Institute, King Mongkut's University of Technology North Bangkok, 1518 Pracharat 1 Road, Wongsawang, Bangsue, Bangkok 10800, Thailand

³ Department of Industrial Engineering and Management, Faculty of Engineering and Industrial Technology, Silpakorn University, Nakhon Pathom 73000, Thailand

*Corresponding author e-mail: jennarong.t@eng.kmutnb.ac.th

Received date:

29 December 2022

Revised date:

6 March 2023

Accepted date:

14 March 2023

Keywords:

Ferritic stainless steel;
AISI 430;
High temperature;
Degradation;
Coal fired boilers

Abstract

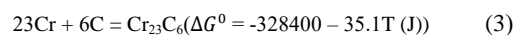
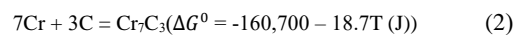
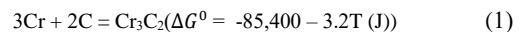
Stainless steel is widely used for many components and parts in coal-fired thermal power plants. AISI 430 ferritic stainless steel (FSS) is one common grade to combat the degradation at high temperatures in coal combustion atmospheres containing flue gas, coal ash, and soot (impure solid carbon particles). However, the effect of the solid carbon particles on the degradation of FSS needs to be clarified. Graphite powder was used to simulate solid carbon atmospheres for investigating the degradation of AISI 430 at high temperatures of 1150°C to 1350°C in coal-fired boilers. After the carbothermic reduction, the mass gain of a pre-oxidized sample at 750°C was approximately 0.0793 mg·cm⁻² and increased when increasing the reduction temperature. The peak of Fe₂O₃ and Cr₇C₃ were detected by X-ray diffraction (XRD) after the oxidation and reduction test, respectively. Besides, the degree of sensitivity (%DoS) of the samples was measured by double loop electrochemical potentiokinetic reactivation (DL-EPR) technique and increased around 30 times after heating the pre-oxidized sample to 1150°C.

1. Introduction

Coal-fired boilers are generally used to turn water into steam by combustion processes and drive an electrical generator for generating electricity in thermal power plants. The high-temperature degradation of steel components can occur in the operating temperature range of 450°C to 1400°C. The main critical problem is fireside corrosion on boiler tube surfaces caused by fuel ash in combustion gases [1-3]. The combustion gas consists of 7.49% to 45% carbon monoxide (CO), 9.0% to 15.28% carbon dioxide (CO₂), 9.5% to 50.5% water vapour (H₂O), and up to 8% flue ash. Soot or impure carbon particles from the flue ash can deposit on the steel surfaces with a particle velocity of less than 20 m·s⁻¹ and lead to the carburization reaction between steel and carbon [2,4].

AISI 430 stainless steel (17%Cr, 0.12%C) is widely used in many applications because of adequate corrosion resistance and good thermal expansion. Besides, it is a low-cost alternative to other stainless steels, but its high-temperature corrosion resistance is lower when compared to austenitic stainless steels (ASS) [5-8]. Using ferritic stainless steel at high temperatures is one possible way to reduce material costs for general stainless-steel components under low aggressive environments in power plants. However, intergranular corrosion and deterioration of passive film may present during the combustion process due to carbon diffusion [9-11]. Solid carbon from soot particles can diffuse

into austenite grain at temperatures between 830°C to 1400°C and form chromium carbide along grain boundaries following Equation (1-3) [5,12,13]. Besides, the chromium oxide film on steel surfaces can decay and transform to chromium carbides as expressed in Equation (4). The chromium carbides of Cr₃C₂, Cr₇C₃, and Cr₂₃C₆ can be formed when the sensitization temperature above 475°C [9,13-15]. They can be predicted using the standard Gibbs free energy free change of chromium carbide formation calculated by thermodynamic data from Kubaschewski [16]. The carbides can cause intergranular corrosion and stress corrosion cracking (SCC) in stainless steel equipment such as boiler tubes and steam turbines in power plants and refineries [17-19].



In this work, the AISI 430 stainless steel was used to study the degradation of ferritic stainless steel in solid carbon atmospheres at 1150°C to 1350°C for 60 min. The graphite powders were used as solid carbon particles in coal-fired boilers and simulated the combustion

atmospheres. The effect of the simulated carburization atmosphere on the degradation of the AISI 430 was observed. The corrosion resistance of the steels can be estimated by the degree of sensitization (%DoS) with the Electrochemical Potentiokinetic Reactivation (EPR) double-loop technique. After the carburization, the microstructure of AISI 430 specimens was observed by a light optical microscope (OM) and a scanning electron microscope (SEM) equipped with energy dispersive spectroscopy (EDS). Finally, the phase analysis was performed by X-ray diffractometer (XRD).

2. Experimental

AISI 430 stainless steel with the chemical composition in Table 1 was used and prepared in a dimension of 20 mm × 20 mm × 5 mm. The samples were polished with 180, 320, 400, 600, 800, and 1000-grit silicon carbide sandpapers. They were then weighed and recorded raw data of the specimens before testing. The specimens were further oxidized in air at 750°C for 48 h to simulate the high-temperature oxidation of FSS at the beginning of the gasification process before the reduction test.

2.1 Reduction test

The pre-oxidized samples were placed into a crucible and covered with graphite powders. Then they were put into a horizontal tube furnace and heated at 1150°C to 1350°C for 60 min, and argon gas was used as shielding gas during heating and cooling. After the reduction test, three different samples were weighed by a 5-digit micro analytical balance to measure the mass change for one condition.

2.2 Materials Characterization

The microstructure of all specimens was observed by a light optical microscope (OM) and scanning electron microscope equipped with energy dispersive spectroscopy (SEM-EDS) (Model QUANTA 450). The SEM was operated in the mode of high-resolution images of shapes of objects (Secondary Electron Image, SEI) and EDS analysis at a voltage of 15 kV. Moreover, the X-ray diffractometer (Model SmartLab), using the incident Cu-K α line, $\lambda = 1.5406 \text{ \AA}$, at 40 kV and 40 mA with the scanning speed of 0.05 deg·sec⁻¹, range angle $2\theta = 20$ to 80 degree and sampling width of 0.02 degree, was conducted for crystal phase identification of AISI 430 samples after the pre-oxidation and reduction tests.

In addition, the samples were etched by waterless Kalling's reagent (1 g Cu₂Cl, 20 mL HCl and 20 mL Ethanol, swab for 3 s to 20 s) for general observation by OM. The carbide formed in the samples was investigated using Murakami's reagent (100 mL water, 10 g NaOH and 10 g K₃Fe(CN)₆, at 80°C for 30 s). The carbide color (M₂₃C₆, M₇C₃, and M₆C) was distinguished by OM and SEM [20]. The hardness of each phase in the microstructure was measured by a Micro-Vickers hardness tester (Digital auto turret, Model 402MVD) with test force of 200 gf.

2.3 Double loop electrochemical potentiokinetic reactivation (DL-EPR) test

Double loop electrochemical potentiokinetic reactivation (DL-EPR) technique was applied to investigate the intergranular corrosion of ferritic stainless steel. The DL-EPR technique was performed by VPM3 potentiostat, using a three electrodes setup in H₂SO₄ electrolyte (1 M) without a depassivator at $17 \pm 3^\circ\text{C}$ [21]. The potential applied from open circuit potential (E_{ocp}) to passivation potential of +200 mV versus SCE (Saturated Calomel Electrode) as a reference electrode. Then the applied potential was reversed to open circuit potential at a scanning rate of 3 mV·s⁻¹. The degree of sensitization (%DoS) was calculated by the current ratio of the reactivation current peak (I_r) and activation current peak (I_a) from a passive state. The assessment of carbide to the %DoS was realized intergranular corrosion (IGC) attack.

3. Results and discussion

The mass gain of AISI 430 samples after the reduction test was measured to investigate the deterioration of the steel samples in the simulated carburization atmospheres. The mass gain of pre-oxidized samples at 750°C was $0.0793 \pm 0.075 \text{ mg}\cdot\text{cm}^{-2}$ and increased linearly by a linear constant of mass gain over reduction temperatures of $3.34 \text{ mg}\cdot\text{cm}^{-2}\cdot^\circ\text{C}^{-1}$ with reduction temperatures (1150°C to 1350°C) as shown in Figure 1. The huge mass change could be from the oxide and carbide formation on the steel surfaces correlating to the work of Penpisuth Thongyong *et al.* [4]. Moreover, the XRD pattern (Figure 2) shows the peaks of iron oxides (Fe₂O₃, ICDD Card No. 24-0072 and Fe₃O₄, ICDD Card No. 75-0449), spinel oxide (CrMn₂O₄, ICDD Card No. 82-0663), and chromium oxide (Cr₂O₃, ICDD Card No. 82-1484) after pre-oxidation at 750°C for 48 h. After the reduction test, the chromium carbide peaks of (Cr₇C₃, ICDD Card No. 36-1482) and (Cr₂₃C₆, ICDD Card No. 35-0783) were additionally presented with

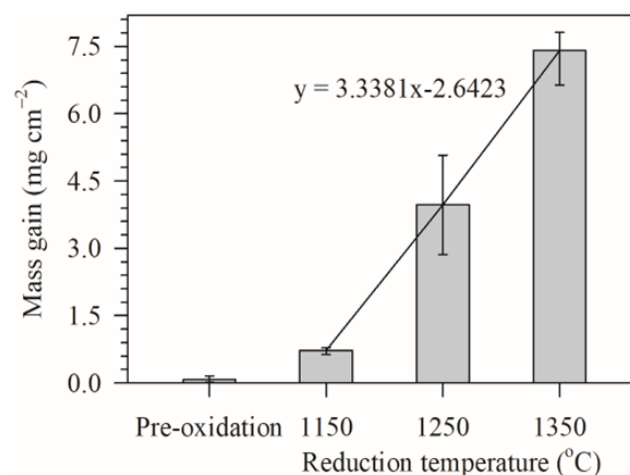


Figure 1. Mass gain of AISI 430 stainless steel after pre-oxidation for 48 h and reduction in graphite powders at different temperatures for 60 min.

Table 1. The chemical composition of AISI 430 stainless steels (wt%) analyzed by optical emission spectroscopy.

Chemical formula	C	Mn	Si	Cr	Ni	Mo	Al	Fe
wt%	0.10	0.79	0.20	16.40	0.05	0.01	0.10	82.23

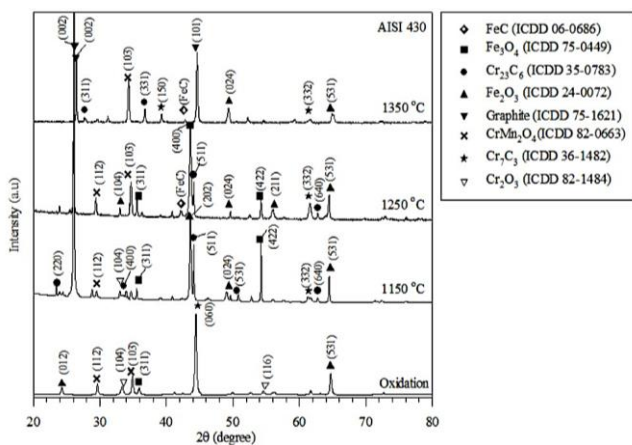
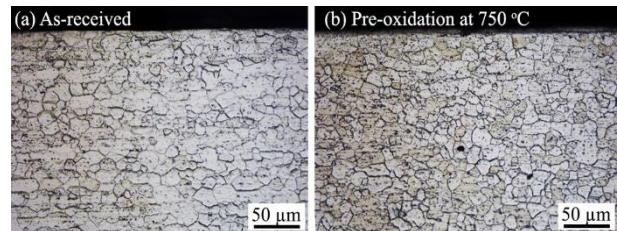
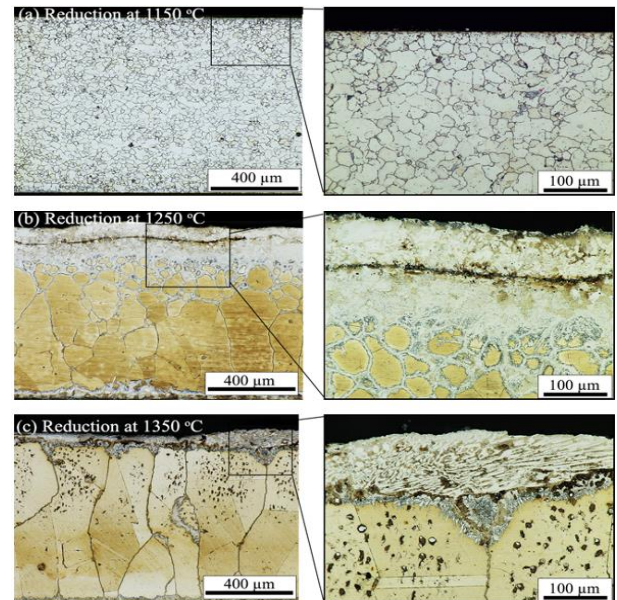
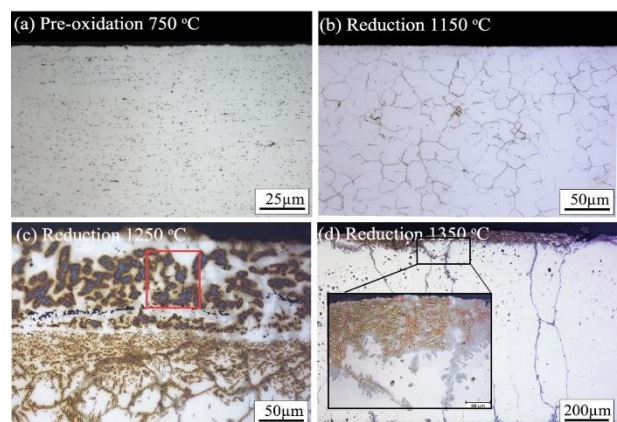
Table 2. The standard Gibbs free energy for the formation of Cr_3C_2 , Cr_7C_3 and Cr_{23}C_6 calculated by Thermodynamics data [16].

Chromium carbide	Equation	ΔG° (J)		
		1150°C	1250°C	1350°C
Cr_3C_2	(1)	-89,953.6	-90,273.6	-90,593.6
Cr_7C_3	(2)	-187,310.1	-189,180.1	-191,050.1
Cr_{23}C_6	(3)	-378,347.3	-381,857.3	-385,367.3

the peak of those oxides. The results can be confirmed the occurrence of oxides and carbides on the stainless steels after the reduction test. The standard Gibbs free energy for the formation of Cr_3C_2 , Cr_7C_3 , and Cr_{23}C_6 from Equation (2-4) can be determined by Thermodynamics data [16] at the reduction temperatures and presented in negative values indicating spontaneity in Table 2.

In Figure 3, the cross-sectional microstructure of as-received and pre-oxidized AISI 430 steel samples showed homogenous white grains of ferrite phase relating to the typical microstructure of AISI 430 [5-7,12]. A continuous network at grain boundaries was presented after pre-oxidation and reduction at 1150°C, as illustrated in Figure 3 and Figure 4(a). Furthermore, the acicular phase was revealed along grain boundaries at the top part of the sample at 1250°C with larger grains and a thick white layer presented on the uppermost. When increasing the temperature to 1350°C, the microstructure surprisingly changed and showed larger grains with twin boundaries and small dark lump phases. Moreover, the acicular phase region decreased, and the white layer showed a two-mixed phase structure of white needles and dark lumps.

The samples were further etched by Murakami's reagent to observe the carbide formation, especially for M_7C_3 and M_{23}C_6 , on the steel microstructure, as shown in Figure 5 and Figure 6. A discontinuous network of carbide was colored and appeared on the microstructure of pre-oxidized specimens, and the carbide network obviously appeared after the reduction at 1150°C. The dark purple-orange lump carbides were inside the top part of the sample at 1250°C, and precipitated orange carbides were inside and along grain boundaries. At 1350°C, the carbides presented as orange needles in the compact two-mixed phases as described above. The dark stained phase around the small lump carbides might be martensite relating to the research of R. Strand *et al.* [22].

**Figure 2.** XRD spectra of AISI 430 stainless steel after pre-oxidation for 48 h and reduction in graphite powders at different temperatures for 60 min.**Figure 3.** Cross-section images of AISI 430 after etching with Kalling's reagent (a) before (b) after exposure at 750°C for 48 h in air atmosphere.**Figure 4.** Cross-section images of AISI 430 after etching with Kalling's reagent (a) after reduction at 1150°C, (b) at 1250°C, and (c) at 1350°C for 60 min.**Figure 5.** Cross-sectional OM (etching with Murakami's reagent) images of AISI 430 after (a) pre-oxidation at 750°C and reduction test at (b) 1150°C, (c) 1250°C, and (d) 1350°C.

The microstructure of those samples was additionally observed by SEM-EDS analysis to verify the type of existing carbides. In Figure 6(b), the high chromium content presented at the grain boundaries (Spot 1) compared to the matrix phase content (Spot 2) for the samples at 1150°C. For the reduced samples at 1250°C and 1350°C in Figure 6(c-d), the carbide micro-islands (Spot 1) on the outermost part (Zoomed area in a red square of Figure 5(c)) showed high chromium contents compared to that of another phase (Spot 2). Thus, the chromium carbides can be formed and related to the dark carbide networks and dark lump carbides, as mentioned in the previous microstructure.

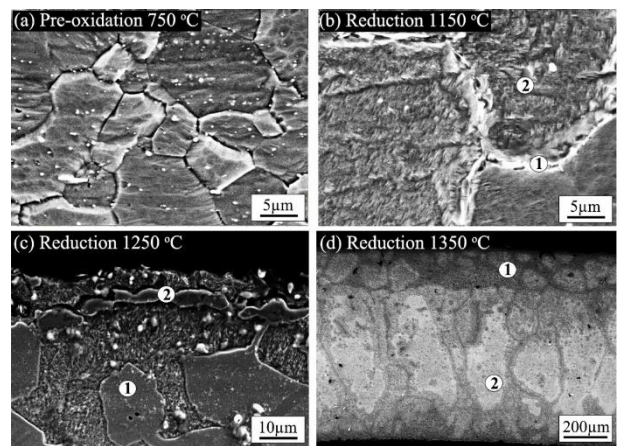
After the characterization, the microhardness measurement was performed and measured from three positions for each phase to validate the phase analysis, as presented in Figure 7. The hardness of the as-received and pre-oxidized samples is 141.4 ± 11 HV and 141.5 ± 4.85 HV, respectively, and it is nearly the hardness of the ferrite phases with 0.7% Ni and 0.6% Cr [7]. In Figure 7, the two-mixed phase structure consisting of small lump carbides (Position 1 and 2 in Figure 7(a)) showed a high hardness of 367.9 ± 19.00 HV and 429.3 ± 22.9 HV, respectively. Likewise, the hardness of the two-mixed phase structure in Figure 7(b) (Position 1) is 424.3 ± 12.65 HV. The hardness of large grains (Position 4 in Figure 7(a) and position 2 in Figure 7(b)) is between 249.1 HV to 280.1 HV relating to the hardness of austenite phases with 18%Cr and 8%Ni [7].

As the results of XRD analysis, microstructure characterization, and hardness test, the phase transformation of AISI 430 stainless steel in the simulated carburizing atmospheres can be explored. The chromium carbide of Cr_7C_3 spontaneously precipitated as discontinuous carbide networks at grain boundaries of the ferrite matrix after exposure at a sensitization temperature of 750°C. This carbide formation correlates with the carbide formation of previous research work [23]. After placing the steel in the carburizing atmosphere of graphite at 1150°C, the carbon can directly diffuse into the steel structure and firmly form chromium carbide as networks along grain boundaries. When the temperature increases to 1250°C, the chromium carbide of Cr_7C_3 and Cr_{23}C_6 are mainly formed as lump phases on the steel surface, next to surrounding graphite atmospheres or called the ‘carburized zone’. Moreover, compact two-mixed phases of chromium carbides and steel matrix occur at the grain boundaries. The chromium carbides can be formed due to the increase of carbon solubility and diffusion from the ambient atmosphere into stainless steel substrate [7,24].

The austenite grains reasonably appear instead of the ferrite grains because of solid carbon powders (austenite stabilizer) supply from the environment and the decrease of chromium content (ferrite stabilizer) from carbide formation. For this reason, the austenite and carbide loop in the Fe-Cr-C diagram (17%Cr stainless steel) can be extended [25,26]. The appearance of austenite phases on the microstructure is in good agreement with the work of R. Strand that presented carbide, austenite, and martensite on the microstructure of 7Cr27Mo2 steels after nitrocarburizing at 440°C for 16 h [22]. The twin boundaries clearly show in the austenite grains, presumably an annealing twin resulting in a change in the crystal system or the arrangement of atoms in one of the grains during cooling [24]. The annealing twin can be generated during recrystallization or grain growth [27]. The austenite grain growth occurs at 1250°C and 1350°C because of high austenitizing temperatures [28]. The precipitated chromium carbides can exist in

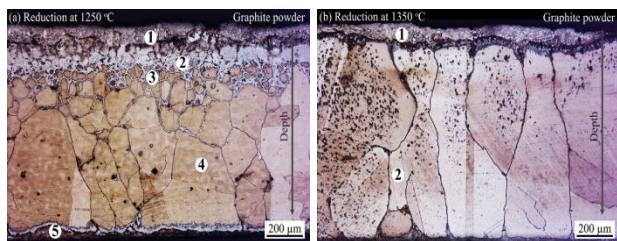
the large austenite grain at 1350°C with high carbon solubility in austenite grains [22].

The intergranular corrosion resistance of the AISI 430 samples before and after the reduction test in carburizing atmospheres was conducted by double-loop electrochemical potentiokinetic reactivation (DL-EPR) analysis. The activation and reactivation current density profiles can indicate intergranular corrosion (IGC) susceptibility. The reformation of the passive film layer can be predicted by the high-skewed reactivation current (I_r) profile, as illustrated in Figure 8(a-c). In addition, the ratio of reactivation and anodic current densities (I_r/I_a) or degree of sensitization (%DoS) in Figure 8(d) is used to determine the IGC susceptibility. The %DoS of as-received specimens is 0.35% which is less than the generally acceptable intergranular corrosion severity of 1.0% [21].



Elements (wt%)	Reduction test					
	1150°C		1250°C		1350°C	
	Spot 1	Spot 2	Spot 1	Spot 2	Spot 1	Spot 2
Cr	25.6	16.4	41.2	40.3	32.7	15.3
C	16.7	13.3	26.0	37.5	35.6	17.3
Fe	57.7	70.3	32.8	22.2	31.7	67.4

Figure 6. Cross-sectional SEM images (etching with Murakami’s reagent) with the corresponding EDS spot elemental analysis of AISI 430 after (a) pre-oxidation at 750°C and reduction test at (b) 1150°C, (c) 1250°C (Zoomed area in a red square of Figure 5(c)), and (d) 1350°C.



Reduction temperature (°C)	Position	Depth* (µm)	Hardness (HV)
1250	1	48.583	367.9 ± 19.00
	2	130.667	429.3 ± 22.9
	3	306.851	303.4 ± 8.75
	4	743.943	249.1 ± 9.45
	5	932.138	248 ± 11.45
1350	1	42.048	424.3 ± 12.65
	2	740.024	280.1 ± 21.60

* Depth from the specimen surface exposed to graphite powder.

Figure 7. Microhardness of the AISI 430 samples at different positions on microstructures after the reduction test at (a) 1250°C and (b) 1350°C.

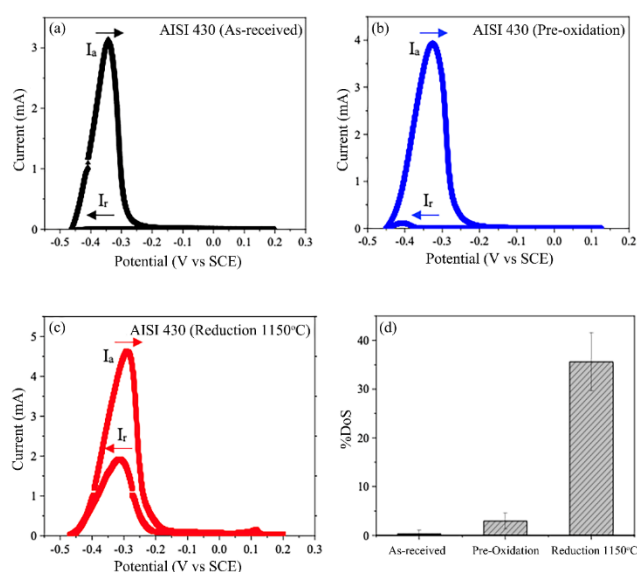


Figure 8. The activation and reactivation current density profile of (a) the as-received AISI 430 specimens (b) after pre-oxidation and (c) reduction test at 1150°C, and (d) the degree of sensitization.

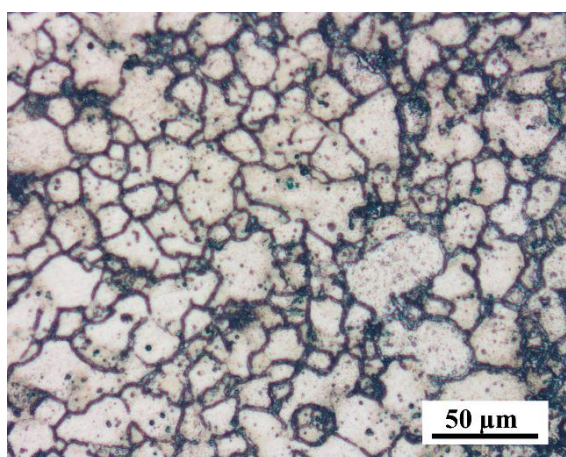


Figure 9. The microstructure of reduced AISI 430 steel at 1150°C after the DL-EPR test.

However, the %DoS of the specimens increased and more than 1.0% after pre-oxidation and reduction. The %DoS of reduced samples increased around 30 times when increasing the temperature to 1150°C. Nevertheless, the DoS test could not perform to investigate the reduced samples at 1250°C and 1350°C because the H_2SO_4 electrolyte was not appropriate to achieve the DL-EPR test for ferritic stainless steel after phase change (ferrite to austenite). The suitable electrolyte is an interesting issue for future studies to obtain the degree of sensitization of those samples. After the DL-EPR test, the passive film breakdown was characterized as presented in Figure 9.

4. Conclusions

- The high deterioration of AISI 430 stainless steel can be predicted by the increasing mass gain with a linear constant of mass gain over reduction temperatures of $3.34 \text{ mg}\cdot\text{cm}^{-2}\cdot\text{C}^{-1}$ after exposure at 1150°C to 1350°C in solid carbon atmospheres.

- The chromium carbide of Cr_7C_3 and $Cr_{23}C_6$ were formed along grain boundaries as networks after the reduction test between 1150°C to 1350°C. This formation plays an important role in intergranular corrosion leading to failures in ferritic stainless-steel structures.
- High carbon diffusion from graphite can promote carbide formation in ferritic stainless steel at high temperatures.
- The high degree of sensitivity of the AISI 430 is around 30 times when heating in the simulated carburizing atmospheres.

Acknowledgements

This research was funded by King Mongkut's University of Technology North Bangkok and National Science and Technology Development Agency, Thailand. Contract no. Grad. 010/2564, and kindly technical supported by Corrosion Technology Department, Thai-French Innovation Institute, King Mongkut's University of Technology North Bangkok.

References

- C. Matthews, *Case Studies in Engineering Design*. Butterworth-Heinemann, 1998.
- G. N. Krishnan, R. Malhotra, J. Perez, M. Hornbostel, K.-H. Lau and A. Sanjurjo, *Diffusion Coatings for Corrosion-Resistant Components in Coal Gasification Systems*. Pittsburgh, PA: U.S. Department of Energy National Energy Technology Center, 2007.
- J. G. Speight, *The refinery of the future*. Cambridge (Mass.), Kidlington: Gulf Professional Publishing, 2020.
- P. Thongyong, S. Chandra-Ambhorn, and J. Tungtrongpairoj, "The degradation of oxide layer on Cr-containing steels in simulated atmospheres on carbothermic reduction," *Materials at High Temperatures*, vol. 39, pp. 1-11, 2022.
- P. Lacombe, B. Baroux, and G. Beranger, *Stainless steels*. France: Les Editions de Physique, 1993.
- D. T. Llewellyn, *Steels: metallurgy and applications*. Elsevier, 1998.
- W. Bleck, *Materials Science of Steel-Textbook for Students at RWTH Aachen*. Steel Institute (IEHK) of RWTH Aachen University, 2016.
- American Iron and Steel Institute, *High-Temperature Characteristics of Stainless Steels*. Nickel Development Institute, 2004.
- P. Thongyong, and J. Tungtrongpairoj, "Carbothermic reduction of the waste chromium oxide rods from thermal spray processes," *IOP Conference Series: Materials Science and Engineering*, vol. 965, pp.12024, 2020.
- P. Treewiriyakitja, P. Thongyong, S. Pokwitidkul and J. Tungtrongpairoj, "The degradation of austenitic stainless steel at high temperature in simulated carbon monoxide containing atmosphere of biomass-to-liquid plants," *IOP Conference Series: Materials Science and Engineering*, vol. 1163, pp. 12022, 2021.
- J. Tungtrongpairoj, P. Thongyong, P. Saranyachot and S. Chandra-Ambhorn, "High temperature degradation of thermal oxides on AISI 304 stainless steels by carbon," *Key Engineering Materials*, vol. 856, pp. 21-28, 2020.

- [12] G. Lothongkum, *Stainless steels*. Chulalongkorn University Press, 2021.
- [13] D. R. Laranjo, "Thermodynamic analysis in the production of chromium carbide from the reduction of chromium oxide with methane-containing gas," *Reactions*, vol. 183, pp. 120-125, 2018.
- [14] B. Leffler, and A. Iversen, "Aqueous corrosion of stainless steel," *Corrosion and Degradation of Engineering Materials*, vol. 3, pp. 1802-1878, 2010.
- [15] D. L. Engelberg, and J. A. Richardson, *Intergranular corrosion*. in Shreir's Corrosion. Elsevier B.V., 2010.
- [16] O. Kubaschewski, C. B. Alcock, *Metallurgical thermochemistry 5th ed.* UK: Pergamon Oxford, 1979.
- [17] K. B. Yoo, Y. He, H. S. Lee, S. Y. Bae, and D. S. Kim, "Study on the microstructural degradation of the boiler tubes for coal-fired power plants," *KEPCO Journal on Electric Power and Energy*, vol. 4, pp. 25-31, 2018.
- [18] F. I. Haider, and M. H. Suryanto, "Carbon diffusion in 304L austenitic stainless steel at 650-750°C in carburizing environment," *International Journal of Recent Technology and Engineering (IJRTE)*, vol. 7, pp. 76-78, 2019.
- [19] H. M. Tawancy, "On the comparative degradation of selected Cr₂O₃-forming alloys by high-temperature carburization with a case study involving 310 stainless steel," *Engineering Failure Analysis*, vol. 110, pp. 104402, 2020.
- [20] G. F. Vander Voort, *Color Metallography*. Metals Park, OH: American Society for Metals, 2004.
- [21] T. Amadou, H. Sidhom and C. Braham, "Double loop electrochemical potentiokinetic reactivation test optimization in checking of duplex stainless steel intergranular corrosion susceptibility," *Metallurgical and Materials Transactions A*, vol. 35, pp. 3499-3513, 2004.
- [22] R. Strand, T. L. Christiansen, and M. A. J. Somers, *M. Sc. thesis*. Technical University of Denmark, 2012.
- [23] M. Romedenne, F. Rouillard, D. Hamon, B. Malard, and D. Monceau, "Carburization of austenitic and ferritic stainless steels in liquid sodium: Comparison between experimental observations and simulations," *Corrosion Science*, vol. 159, p. 108147, 2019.
- [24] H. K. D. H. Bhadeshia and R. W. K. Honeycombe, *Steels microstructure and properties (Third edition)*. Butterworth-Heinemann, 2017.
- [25] A. G. Andreeva, and A. P. Gulyaev, "Carburization of stainless steels," *Metal Science and Heat Treatment of Metals*, vol. 2, pp. 137-140, 1960.
- [26] S. Kou, and Y. Le, "The effect of quenching on the solidification structure and transformation behavior of stainless steel welds," *Metallurgical Transactions A 13*, vol. 7, pp. 1141-1152, 1982.
- [27] G. Gottstein, *Physical foundations of materials science*. Springer-Verlag Berlin Heidelberg GmbH, 2004.
- [28] A. K. Sinha, *Ferrous physical metallurgy*. Boston (Mass.): Butterworths, 1989.